# Local climatological modeling of ionospheric irregularities detected by GPS in mid-latitude region

G. Wautelet[1,*], R. Warnant[1]

[a]*Geomatics Unit, University of Liege, 17 Allee du 6 Aout (B5a), B-4000 Liege, Belgium*

**Abstract**

Global Positioning System, or GPS, plays an important role in everyday life. More particularly, precise positioning applications constitute a continuously growing sector whose surveyors, civil engineers and more recently farmers represent the principal users. Ionospheric irregularities are considered as the main threat for those applications as their occurrence and their effects on positioning are generally unknown or unmodeled. This paper aims at setting up a local climatological model of such irregularities which can be used as a forecasting tool. The model is based upon a time series of GPS-derived ionospheric irregularities in Belgium covering ten years of data (period 2002-2011). Our climatological model is twofold: its first component describes the daily variability and is derived from a principal component analysis (PCA) which allows to retrieve the main patterns of the time series. With the use of low order polynomial and harmonic functions, the second component describes the influence of solar cycle and seasons on irregularity occurrence. Moreover, a statistical autoregressive formulation adapts the model to current conditions. Model validation covers both low and active solar activity periods (years 2008 and 2011) and shows that model accuracy varies with solar conditions and season: values are lower during winter and active solar activity periods, where modeling error can reach up to 60% of the observed value. During summer, model performance is clearly improved, with relative errors generally smaller than 20% for periods of low but also active solar activity.

*Keywords:*
Ionosphere, GPS, Climatology, Modeling

## 1. Introduction

Global Positioning System, also known as GPS, is part of in everyday life and is more and more used in precise navigation. More particularly, one could observe an increasing number of users of relative positioning techniques. These techniques allow the user to measure its position with respect to a reference station for which the position is accurately known. Because measurements are relative, all errors common to the two stations cancel out and the final precision of the user coordinates is about a few centimeters (Leick, 2004; Hofmann-Wellenhof et al., 2001; Xu, 2003). Among these errors is the ionospheric one which is proportional to the Total Electron Content (TEC), defined as the integral of the free electron density along the satellite to receiver path. In the frame of relative positioning, this error is said to be residual as we are dealing with relative measurements. The cm-level accuracy of the technique is reached if the ionospheric residual term can be neglected, which happens on two conditions: the baseline between the stations should be small (ideally shorter than 20 km) and the ionosphere must be quiet and regular. These two conditions express a strong spatial and temporal autocorrelation of the ionosphere, and more particularly of the vertical TEC (Kutiev et al., 1999; Muhtarov and Kutiev, 1999). This leads to insure that two measurements close to each other are strongly correlated so that their TEC difference can be assimilated to the noise level.

Ionospheric irregularities are seen as irregular gradients in the plasma and their origin is twofold: space-weather events and lower atmosphere. The first is responsible for the most severe irregularities and includes two main phenomena: solar flares (X and EUV rays) and geomagnetic storms resulting from interactions be-

*Corresponding author. Tel.: +32 4 366 57 44 ; fax: +32 4 366 56 93

*Email addresses:* gilles.wautelet@ulg.ac.be (G. Wautelet), rene.warnant@ulg.ac.be (R. Warnant)

tween coronal mass ejections (CME) and the geomagnetic field. The related ionospheric gradients of several TECu (1 TECu = $10^{16}$ electrons/m$^2$) may induce positioning errors up to several meters for a relatively short baseline of about 10 km (Lejeune and Warnant, 2008; Lejeune et al., 2012).

Although they are responsible for large amplitude irregularities, space-weather events occur less often than medium-scale traveling ionospheric disturbances (MSTIDs). Identified as the second cause of irregularities, they constitute the major part of irregularities detected over mid-latitudes (Wautelet et al., 2009). MSTIDs, with periods ranging from 10 minutes to 1 h (Georges, 1968; Hunsucker, 1982) are considered as the signature of atmospheric gravity waves (AGWs) into the ionospheric plasma, this latter playing the role of a passive tracer. AGWs are mainly generated by neutrospheric variability (Lastovicka, 2006) and more particularly by phenomena of meteorological origin, like jet stream (Bertin et al., 1978), wind shears and orography (Hocke and Schlegel, 1996) or storms and front systems. Earthquakes constitute another source of AGWs and are called ionoquakes if they exhibit a signature in the ionosphere (Rishbeth, 2006).

Before the advent of GPS, all climatological and morphological studies came from ground-based observations, such as VLF transmission links, ionospheric sounders or scatter radars. Nowadays most of ionospheric studies are based on TEC derived from GPS measurements (Hernandez-Pajares et al., 2006; Kotake et al., 2006; Kouris et al., 2006). However, they do not provide any climatological model of irregularity occurrence that can be useful for GPS high-end users. As a matter of fact, there is a growing interest of such users to be aware, if possible in advance, of threats due to ionospheric irregularities on their position computation. This point becomes more and more important as next solar maximum comes closer and as GPS users community is still expected to grow.

In this paper we present an original technique to analyze an ionospheric irregularity time series covering ten years of GPS data in Belgium. We use a principal component analysis (PCA) to extract the most regular patterns from the series and build a local climatological model based on a limited number of principal components coming from the PCA. In section 2 we explain the methodology used: after the retrieval of the ionospheric irregularity time series, the principles relative to its analysis are described. In section 3, PCA results are detailed and lead to the elaboration of a PCA model representing the most recurrent daily patterns in the series. Furthermore, a second model based on harmonic decomposition and autoregressive functions has been developed to take into account of the day-to-day mean level, which is mainly due to secular variations of solar conditions. The final model, called climatological model, is then computed as the sum of these two models and validated over low and active solar activity periods. This final model can be considered as a local model since its computation and validation have been achieved based on Belgian data only.

## 2. Methodology

The climatological study presented in this paper relies on a data set covering ten years of GPS data in Belgium. The first part of this section describes the ionospheric irregularity detection using GPS measurements and the setting up of its associated time series. In a second part the main concepts of the principal component analysis (PCA) are explained, followed by the reconstruction technique based on a subset of principal components.

### *2.1. Ionospheric irregularity detection by GPS: setting up the time series*

GPS satellite broadcast consists in two L-band carriers modulated by ranging codes and navigation signals. To monitor the ionosphere at a given GPS station, it is necessary to have at one's disposal the observations relative to the two frequencies $f_1$ and $f_2$, called respectively $L_1$ and $L_2$. We are then able to extract the slant total electron content (STEC) for a given satellite-receiver pair, which is defined as the integral of the free electron density along the satellite to receiver path. In the case of phase measurements, STEC computation is achieved using the "Geometry-Free" (GF) combination of phase observations:

$$\begin{aligned} \varphi_{GF} &= \varphi_1 - \frac{f_1}{f_2}\varphi_2 \qquad \text{[cycles]} \\ &= \alpha\,\text{STEC} + M_{GF} + N_{GF} + \varepsilon_{GF} \end{aligned} \tag{1}$$

with

- $\varphi_i$ the phase measurement made on frequency $f_i$, expressed in cycles;
- $f_i$ the GPS frequency, with $f_1 = 1\,575.42$ MHz and $f_2 = 1\,227.60$ MHz;
- $\alpha$ a numerical coefficient;
- $M_{GF}$ the multipath term in the GF combination;

$N_{GF}$ the ambiguity term in the GF combination. It represents an unknown non-integer number of cycles.

$\varepsilon_{GF}$ the noise term in the GF combination.

STEC accuracy is about several TECu, which is the order of magnitude of ionospheric irregularities (Warnant and Pottiaux, 2000). To circumvent this difficulty, ionospheric irregularities are detected using STEC temporal differences, which are much more accurate than absolute values. Considering a cut-off elevation angle of 20° and a sampling rate of 30 s, multipath, noise and other elevation-dependent effects can be neglected with respect to ionospheric effect and, as long as the ambiguity term $N_{GF}$ remains the same (*i.e.* no cycle slip), Eq. (1) can be adapted as follows:

$$\begin{aligned} \Delta\text{STEC} &= \frac{\text{STEC}(t_k) - \text{STEC}(t_{k-1})}{t_k - t_{k-1}} \\ &= 1.812\ \frac{\varphi_{GF}(t_k) - \varphi_{GF}(t_{k-1})}{t_k - t_{k-1}} \end{aligned} \quad (2)$$

with $t_k$ and $t_{k-1}$ two adjacent observation epochs.

As STEC values are slant measurements, they have to be mapped to vertical:

$$\Delta\text{VTEC} = \Delta\text{STEC} \,.\, \cos(z_{IPP}) \quad (3)$$

with $z_{IPP}$ the zenithal angle of the satellite at the ionospheric pierce point (IPP), which corresponds to the intersection between the satellite to receiver path and the ionospheric thin shell at 400 km.

Low frequency changes in TEC mainly related to satellite orbital motion can accurately be modeled by a second order polynomial. Residuals of this fit, which will constitute the basis of our study, are called "Rate of TEC" (RoTEC) and are expressed in TECu/min. Then, we compute the standard deviation of RoTEC every 15 min time interval to get $\sigma_{\text{RoTEC}}$ for every satellite in view, which corresponds to ionospheric high-frequency variability and what we will further refer to as "ionospheric irregularities". The sampling rate of GPS measurements being 30 s, each standard deviation value is based on 30 observations. As we observe several GPS satellites at the same time, we average out all $\sigma_{\text{RoTEC}}$ values occurring simultaneously. Moreover, we also use observations related to three Belgian EUREF stations: BRUS (50°47'N, 04°21'E), DENT (50°56'N, 03°23'E) and DOUR (50°05'N, 04°35'E). These stations being relatively close from each other (distance between them ranges from 70 to 125 km), $\sigma_{\text{RoTEC}}$ values are highly correlated and averaging these three measurements provides a reliable series without any data gap and minimize the influence of multipath and possible outliers. The time span analyzed in the frame of this article extends from January 2002 to December 2011, which covers the declining phase of solar cycle 23 and the rise of cycle 24.

Finally, a weighted moving average has been applied to the whole series to minimize the noise level and highlight the ionospheric signal. The sample window covers 45 minutes on each side of the central value, what corresponds to three observation epochs. The time series, further referred to as $\overline{\sigma_{RoTEC}}$, is depicted together with the monthly sunspot number in figure 1. One can observe that the amplitude of irregularities are in phase with solar activity, showing a maximum around 2002 and a long minimum in 2008-2009. Let us also note the rapid rise of solar cycle 24 at the end of 2011, imitated by the irregularity time series. Seasonal patterns can also be identified: large irregularity values occur mostly during winter while few of them take place in summer. We can also observe some peaks, especially in late 2003: these outliers correspond to high ionospheric variability periods due to powerful geomagnetic storms. As a matter of example, the maximum RoTEC value observed at BRUS station during November 20th 2003 storm (DOY 324/03) was about 10 TECu/min, which represents an extremely high variability value for mid-latitude regions. A deeper analysis of the series, although impossible to discriminate from figure 1, concerns daily variability. Two main patterns have been identified: a rise of variability during winter daytime and in the late afternoon (around 8 P.M.) during summer. These climatological features have been quite well described in Wautelet et al. (2009) and will be examined in details in the next section.

In the next paragraphs we carefully analyze the $\overline{\sigma_{RoTEC}}$ time series to retrieve and detail its main climatological patterns.

### *2.2. Time series analysis and PCA*

The most common technique used in time series analysis is the well-known Fourier transform, which allows to identify the most important periods in the series with their associated amplitude. In this paper, we present another way to extract such information: the principal component analysis (PCA), also known as empirical orthogonal function (EOF) analysis. This method has already been successfully used to summarize long time series or to forecast ionospheric parameters such as $f_O F_2$ (Wintoft and Cander, 2000; Collier, 2009). PCA

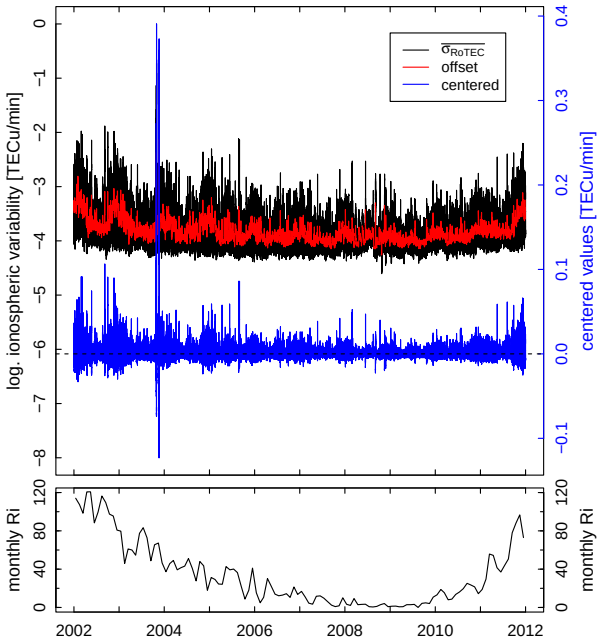


Figure 1: *Top panel:* $\overline{\sigma_{RoTEC}}$ and offset time series. Both series have been log-transformed because of the dynamics of the values. The centered series, which corresponds to $\overline{\sigma_{RoTEC}}$ subtracted by the offset, is depicted with a normal scale. *Bottom panel:* monthly sunspot number *Ri*.

is a multivariate analysis which consists in transforming an original space of correlated variables into another space of uncorrelated variables, called principal components (PC). After this change of base, the greatest part of the information contained in the original space can be summarized using a few PCs only, others being considered as noise. The limited number of dimensions allows therefore an easy interpretation of data features.

In the frame of this paper, the 3652 days constituting the $\overline{\sigma_{RoTEC}}$ time series are considered as the correlated variables and the 96 quarter-hours play the role of the observations. By doing this way, the goal is the analysis of similar daily patterns in order to retrieve the most typical patterns of the series. The original time series is therefore reshaped in a matrix whose structure is shown in table 1.

A preliminary step to PCA is to translate the origin of the observations to their centroid, what will ease PCA processing. In this context, the transformation consists in subtracting the mean for each of the columns to obtain centered values. From now, the series is then divided into two components: the first corresponds to the centered values on which the PCA will be applied and the second is the daily mean series, what will be referred to as "offset" series. Let us mention that the length of

| | 01/01/02 | 01/02/02 | ... | 12/31/11 |
|---|---|---|---|---|
| 00:00 | 0.023 | 0.057 | ... | -0.004 |
| 00:15 | 0.023 | 0.064 | ... | -0.004 |
| 00:30 | 0.023 | 0.070 | ... | -0.005 |
| ... | ... | ... | ... | ... |
| 23:45 | 0.052 | 0.018 | ... | -0.005 |

Table 1: Original time series of $\overline{\sigma_{RoTEC}}$ reshaped in a matrix form containing 96 rows and 3652 columns, corresponding respectively to the quarter-hours and the days.

the offset series is 96 times shorter than that of the centered series, as we have only one value per day. Summing these two components leads to the original series $\overline{\sigma_{RoTEC}}$. Both original and offset series are shown in figure 1 where we can observe solar cycle influence and seasonal patterns in the offset series. In its matrix form, centered series will be referred to as $A$.

The inertial matrix used in PCA algorithm must contain all the redundant information that will be summarized in a few PCs. In this paper the correlation matrix $C$ has been chosen to play that role.

PCA consists in computing the 3652 eigenvectors $X_i$, which will be referred to as principal components (PC), and their associated eigenvalues $\lambda_i$ of the inertial matrix $C$:

$$C\,X_i = \lambda_i\,X_i \tag{4}$$

Each PC is associated to a percentage of the total variance $\sigma^2_{tot}$ contained in the inertial matrix, $\sigma^2_i$, which represents the fraction of the total variance explained by the $i$th PC:

$$\sigma^2_i = \lambda_i/\sigma^2_{tot} = \lambda_i/tr(C)\ \ [\%] \tag{5}$$

with $tr(C)$ the trace of the correlation matrix $C$, which corresponds to the matrix dimension (*i.e.* 3652).

Generally PCs are sorted in order of decreasing importance, so that we can easily identify the few ones which represent the bulk of the total variance. Others can be associated with noise as they represent a small part of the signal. PCs consist in linear combinations of the original variables and their correlations with these variables are called "loadings".

The coordinates of the observations into the new space formed by the PCs are called "scores" and their computation is done through Eq. (6):

$$S' = X'\,A' \tag{6}$$

with

$S'$ the transpose of the scores matrix $S$;

$X'$ the transpose of the principal components matrix $X$, set up by all PCs arranged in columns;

$A'$ the transpose of matrix $A$.

Original data retrieval is achieved by inverting Eq. (6) and $X$ being an orthogonal matrix, we have $X'^{-1} = X$ so the inversion takes the following form:

$$A' = X\,S' \tag{7}$$

As the aim of PCA is to reduce the number of dimensions, it is usual practice to keep only PCs which have been associated with signal pattern; others are considered as non-significant since they correspond to noise. Matrix $X$ is therefore constituted with only a small number of columns and $X$ becomes a (3652 x $n$) matrix, with $n$ the number of PCs kept. We also have to truncate the $S$ matrix on the same way to select only scores relative to the $n$ PCs chosen. These truncations make the Eq. (7) compatible again and we are able to reconstruct the data in the original space. The loss of precision is proportional to the percentage of variance lost by not considering all PCs in the computation.

The reconstruction based on a small number of PCs has the advantage to extract the most recurrent patterns present in the original signal and to keep away the signature of transient events, such as the effects of geomagnetic storms.

As the rest of the methodology follows from results, it will be explained and discussed in the next section. The processing diagram shown in figure 2 depicts the methodology used in this paper.

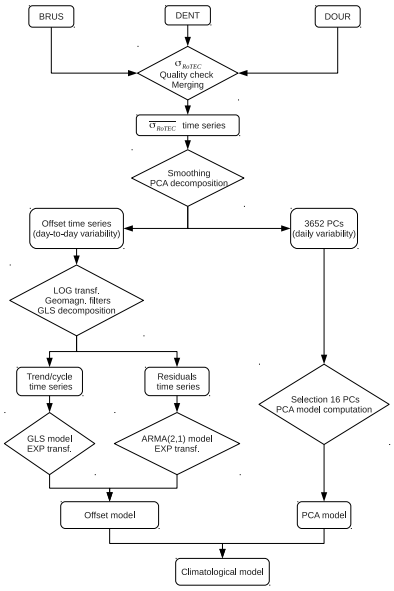


Figure 2: Processing diagram. Data are represented as boxes while methods and transformations are contained in diamonds.

## 3. Results

In a first part, we present the principal component analysis of $\overline{\sigma_{RoTEC}}$ series whose results led to a daily variability model, further referred to as "PCA model". Next, we tackle the setting up of the model related to the offset series (daily means) which, once added to the PCA model, defines the final "climatological model". Lastly, performance of this model is assessed through a validation step considering data related to low and active solar activity periods.

### *3.1. PCA results*

PCA on centered series leads to 3652 PCs whose the ten most important are displayed in table 2, sorted by decreasing percentage of the explained total variance.

In figure 3, cumulative explained variance is plotted with respect to the number of PCs considered. Together

| PC | $\lambda_i$ | $\sigma_i^2$ [%] | $\sum \sigma_i^2$ [%] |
|---|---|---|---|
| 1 | 1215.69 | 33.29 | 33.29 |
| 2 | 676.12 | 18.51 | 51.80 |
| 3 | 287.91 | 7.88 | 59.69 |
| 4 | 270.67 | 7.41 | 67.10 |
| 5 | 183.99 | 5.04 | 72.13 |
| 6 | 138.35 | 3.79 | 75.92 |
| 7 | 129.40 | 3.54 | 79.47 |
| 8 | 115.80 | 3.17 | 82.64 |
| 9 | 84.14 | 2.30 | 84.94 |
| 10 | 82.19 | 2.25 | 87.19 |

Table 2: Eigenvalues, explained variance and cumulative explained variance (expressed in %) for the first ten principal components.

with the analysis of table 2 we can state that the first two PCs represent most of the regular patterns contained in the series, despite a cumulative variance of only ~52%. This relatively weak value is likely associated with the smooth character of $\overline{\sigma_{RoTEC}}$ series (see previous section). To confirm these hypothesis, PCA was also performed on the centered series before being smoothed by the moving average: percentages of explained variance for the first three PCs were respectively 23.8%, 12.5% and 5.5% for a cumulative value of 41.7%. Comparison between these percentages and values displayed in table 2 shows that smoothing is needed if one wants to get the most significant PCs in terms of explained variance.

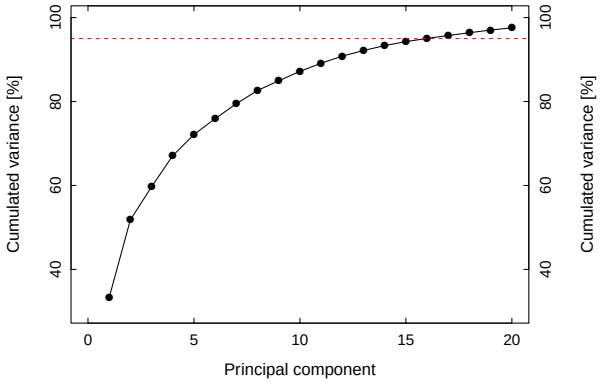


Figure 3: Cumulative explained variance as a function of PC. The dotted line corresponds to the 95% threshold.

Scores and loadings relative to the first four PCs are depicted in figures 4 and 5. Their analysis reveals different patterns essentially associated to the first three PCs.

PC1 presents a scores pattern clearly identified as a 24-hour cycle, due to day-night alternation. It shows a sharp decrease in $\overline{\sigma_{RoTEC}}$ before noon and an increase a bit longer in the afternoon, which is contrary to the quick analysis done when presenting the series (see section 2.1). Having a closer look to the associated loadings we can observe a very strong negative correlation (near -1) during winter days and a rather weak correlation (around 0.5) during summer. The behavior of this PC1 corresponds therefore to an increase of ionospheric variability during daytime in winter, between approximately 8 A.M. and 4 P.M. During nighttime, variability remains more or less constant, with values around 0.15 TECu/min. It is worth noting that this pattern represents about one third of the total ionospheric variability ($\sigma^2_{PC1} \approx 33\%$).

PC2 scores show an asymmetrical pattern: activity decrease between midnight and 8 A.M., followed by a nearly null value during daytime to end with a peak around 8 P.M. Correlations are strong to very strong (0.8-0.9) during summer days, meaning that an increase of evening ionospheric variability in summer is another recurrent pattern in our time series. During winter, days do not seem to respond to PC2 quite well as the correlation values are very variable, reaching sometimes 0.9 but oscillating around zero on average. The periodicity in loadings is once again annual.

Scores relative to PC3 show a cyclic signal with a period of about 12 hours: the two crests of activity occur around noon and 11 P.M. The series of loadings still consists in an annual cycle but shows sharp transitions around fall equinoxes while a large variability around spring equinoxes can be observed in the correlations. In summer, where correlations are rather negative (around -0.5), this PC can be translated as pre-sunset and pre-sunrise bursts of ionospheric activity. During winter months correlations are rather positive (around 0.5) and PC3 not only strengthens the noon peak related to PC1 but also adds a secondary peak around midnight. Moreover, PC3 tends to lower the activity level during the early hours and in the late afternoon.

Loadings of all other PCs are similar to that of PC4 (see figure 5): no clear pattern in correlations can be observed, which makes the interpretation of these components very difficult. To summarize, when considering the first three significant PCs, winter recurrent pattern corresponds to a peak of irregularities around noon probably linked to sunshine duration. A more detailed analysis of PC1 scores shows that peak slopes are not identical: a rapid rise is observed between 7 and 11 A.M. while the decay period in the afternoon takes more time (between noon and 6 P.M.). It is interesting to note that this behavior is quite similar to vertical TEC daily curve at mid latitudes.

### *3.2. Reconstruction and PCA modeling*

We have seen that the first three PCs were responsible for about 60% of the total variance. However, it is usual practice to reconstruct 95% of this original variance. We need therefore to include some non-significant PCs to reach this threshold. According to figure 3, we will use the first 16 PCs to reconstruct the data; the differences

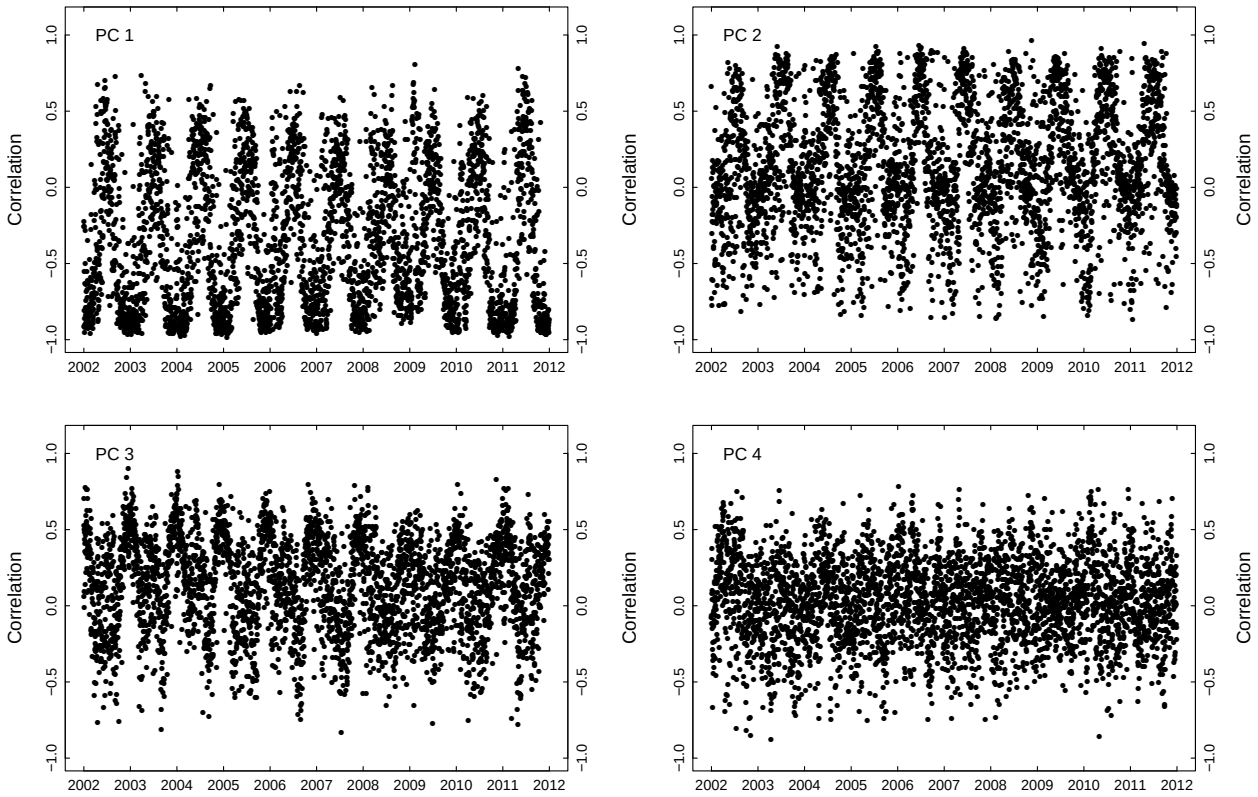


Figure 5: Loadings for the first four PCs.

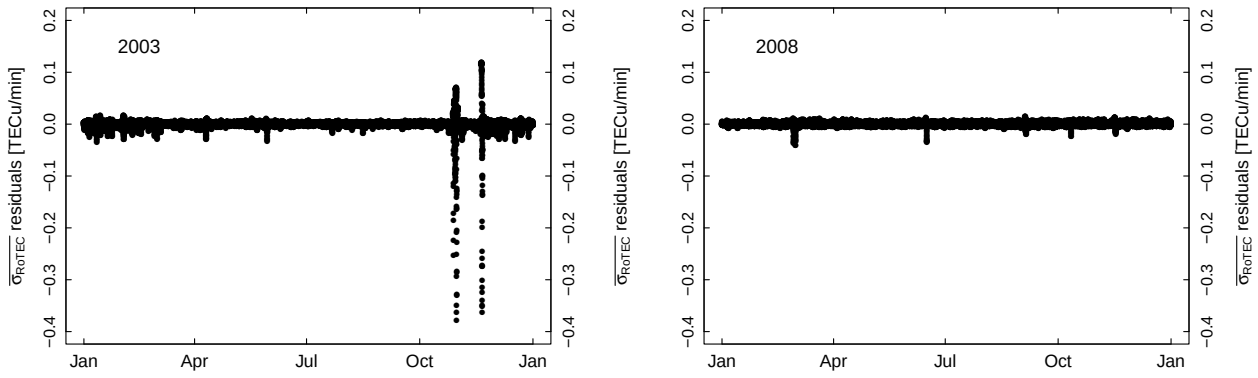


Figure 6: Residuals of PCA reconstruction considering the first 16 PCs for years 2003 (left) and 2008 (right).

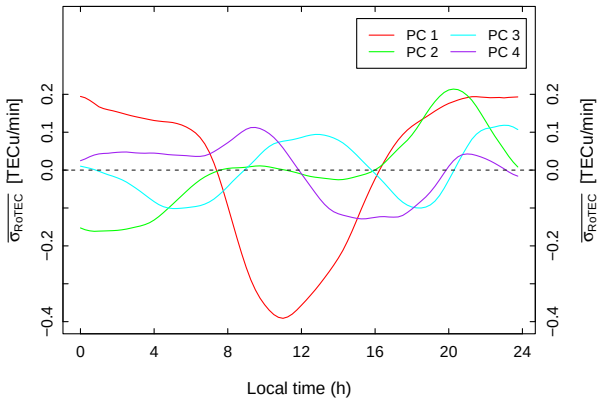


Figure 4: Scores for the first four PCs.

between original and reconstructed data, called residuals, are presented for years 2003 and 2008 in figure 6.

The main feature in figure 6 is the presence of large residuals for specific days, especially for year 2003: these are due to large RoTEC values observed during geomagnetic storms. In that sense, we can confirm that PCA reconstruction allows to identify and filter out all days whose daily behavior differs significantly from typical patterns. Analysis of figure 6 also shows that, for year 2003, residuals are larger in winter than for the rest of the year, which means that winter days differ on average more from PCA regular pattern than other periods of the year. This is probably due to a) high solar activity conditions in terms of extreme-UV radiation and b) winter anomaly, which makes TEC annual maximum occur in winter, despite of a smaller ion production rate than during summer (Davies, 1990). In 2008 (low solar activity period), PCA reconstruction seems to give uniform residuals along the whole year, as geomagnetic storms were rarely occurring and TEC values were usually not larger than 10 TECu.

In this paper, we will use PCA results to build an annual model of centered values. This model will result from averaging several years of data to obtain smooth and continuous daily patterns. Validation will be performed over low and active solar activity periods (see section 3.4). Therefore, two different PCA models will be built and validated separately. For validation during solar minimum (year 2008), PCA model will be based upon periods 2002-2007 and 2009-2011 while validation during active solar conditions (year 2011) will use a model built from 2002-2010 period.

Analysis of figure 5 shows that loadings relative to the first three PCs do not vary much with solar cycle. This is due to the fact that these results are related to centered value and that most effects due to solar cycle (as well as part of seasonal pattern) have already been taken into account when computing the offset series (see section 2.2). The annual cycles in loadings can therefore be averaged to get an eigenvector matrix $X$ of size (365x16). Scores matrix $S$ being already truncated to the first 16 PCs, the reconstruction can be achieved and the result is called "PCA model". This model corresponds to a (96x365) matrix giving centered $\overline{\sigma_{RoTEC}}$ every 15 min for a mean year.

As a matter of example, the comparison between the PCA model built over 2002-2010 and the original centered values is illustrated in figure 7. We can observe that climatological features which have been identified in the previous sections are correctly reproduced in this model: a main rise during winter daytime and a small peak in the late afternoon for summer days. Data related to 2002 show the largest variability with respect to the model: that is a direct consequence of high solar activity encountered in 2002. Considering periods of moderate or low solar activity, one can notice that the PCA model is in good agreement with data. Since an important part of solar cycle influence has been removed by the use of centered values, the PCA model can be repeated from year to year to forecast daily variability due to ionospheric irregularities.

### *3.3. Offset time series modeling*

The PCA model has to be added to the offset time series model to create the final climatological model (see figure 2). As the goal is to retrieve and model the main patterns, we also need to exclude geomagnetically active periods from our series, which can be clearly identified as spikes in figure 1. This is done through the use of geomagnetic indices: criteria used in the frame of this paper are Kp<4 and DST>-50nT. The use of both indices is justified as some irregularities occur during geomagnetic storms recovery periods, for example when Kp value is small but DST index is still recovering to normal conditions.

As for the PCA model, two offset models will be computed in order to validate the method over two different years corresponding to different solar conditions. The model based on 2002-2007 period will be validated on year 2008, during solar minimum. The validation of the active solar activity period will be performed over the year 2011, the related model being derived from 2002-2010 period.

Figure 1 shows that offset variability in not constant with time: variance during low solar activity periods (2008-2009) is clearly smaller than variance during solar maximum (2002). Stabilization is achieved through log-transformation (natural logarithm) of the

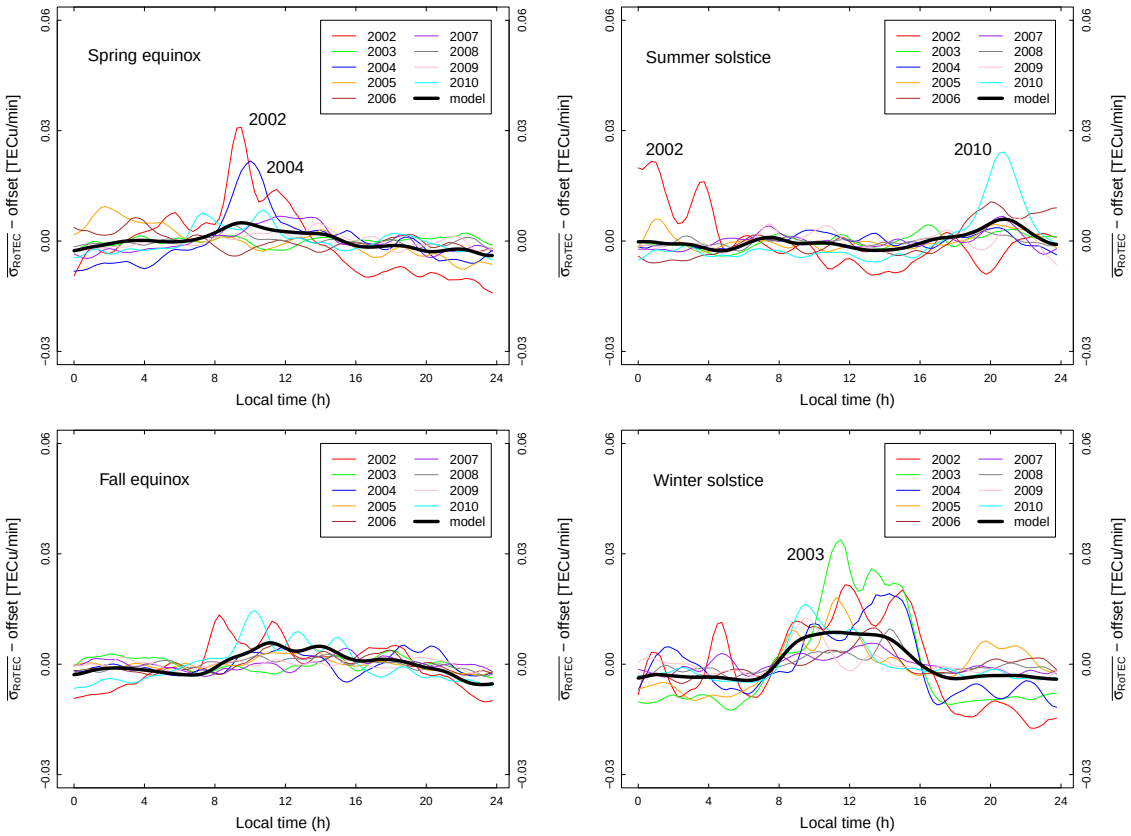


Figure 7: Comparison between original (centered) data and the PCA model for solstices and equinoxes.

series, which gives a steadier series also depicted in figure 1. This transformation will ease model processing, which can be divided into two main steps:

1. Modeling of annual cycle(s) and long-term trend due to solar activity in a least-squares adjustment. The model coming from this procedure is purely mathematical, resulting in a very simple forecast computation.
2. Modeling of the residuals coming from the least-squares adjustment processed in the first step. As this time series is more or less similar to a noisy pattern, specific statistical tools have to be applied for modeling purposes.

### *3.3.1. Modeling trend and cycles: generalized least-squares*

Time series analysis suggests lots of ways for extracting trends and cycles: exponential smoothing, Holt-Winters method, additive and multiplicative decompositions, least-squares method (Cowpertwait and Metcalfe, 2009; Brockwell and Davis, 2002). Many of them have been investigated and the method presented in this paper is the one giving the most satisfactory results. The shape of log-transformed offset series suggests to model the trend with a low order polynomial while cycles can be reproduced with harmonic functions. To accurately model the solar cycle influence, a third order polynomial trend has been chosen. To retrieve frequencies of the series, a Fourier transform is applied to the detrended offset series and detects periods of 182.5 and 365 days, as expected. Annual and semi-annual periodicity, added to the long-term trend can therefore be modeled as follows:

$$\begin{aligned}\text{Offsets}(t) \quad = \quad & a_0 + a_1 t + a_2 t^2 + a_3 t^3 + a_4 \sin\left(\frac{2\pi t}{T_1}\right) \\ & + a_5 \cos\left(\frac{2\pi t}{T_1}\right) + a_6 \sin\left(\frac{2\pi t}{T_2}\right) \\ & + a_7 \cos\left(\frac{2\pi t}{T_2}\right) \end{aligned} \tag{8}$$

with

$a_i$ some numerical coefficients to be computed from the least-squares procedure;

$T_1$ and $T_2$ the two harmonic periods, respectively 182.5 and 365 days.

Partial autocorrelograms obtained from offset time series show strong autocorrelation within the series and, from a statistical point of view, an ordinary least-squares procedure is not suitable in this case. To take this autocorrelation into account, we first need to assess it and then feed a generalized least-squares adjustment (GLS) with such information. Autocorrelation is estimated by fitting the series with a first order autoregressive model - AR(1) - whose principles can be summarized as follows: an observation made at epoch $t$ can be expressed as a fraction of the previous observation added to a white noise term $\varepsilon_t$ : $A_t = \alpha A_{t-1} + \varepsilon_t$. AR(1) model leads to $\alpha = 0.85$, that corresponds to strong autocorrelation, and GLS fitting can therefore be computed using this information. As details of the computing method are out of the scope of this article, we invite the interested reader to consult the following references: Box and Jenkins (1976); Brockwell and Davis (2002).

GLS fitting described in Eq. (8) leads to three coefficients $a_3$, $a_4$ and $a_6$ statistically non-significant as their value is not statistically different from zero. Trend formulation is thus simplified by a second order polynomial and the cycle component relies on a pure cosine model nearly in phase with winter/summer alternation. Eq. (8) can therefore be simplified as:

$$\begin{aligned} \text{Offsets}(t) &= a_0 + a_1 t + a_2 t^2 + a_3 \cos\left(\frac{2\pi t}{T_1}\right) \\ &\quad + a_4 \cos\left(\frac{2\pi t}{T_2}\right) \end{aligned} \tag{9}$$

Data and GLS model are both depicted in figure 8 where extrapolation (forecast) for year 2011 and its related confidence interval are depicted. A more detailed view of 2011 (active conditions) and 2008 (low solar activity) forecasts is depicted in figures 9 and 10, where we can observe the increase due to the polynomial model, translating the rising activity of solar cycle 24.

### 3.3.2. *Modeling residuals: ARMA model*

Subtracting the GLS model from the offset observations leads to the residual time series depicted in figure 8. Although this series presents a null mean average, we can identify some periods where values do not vary

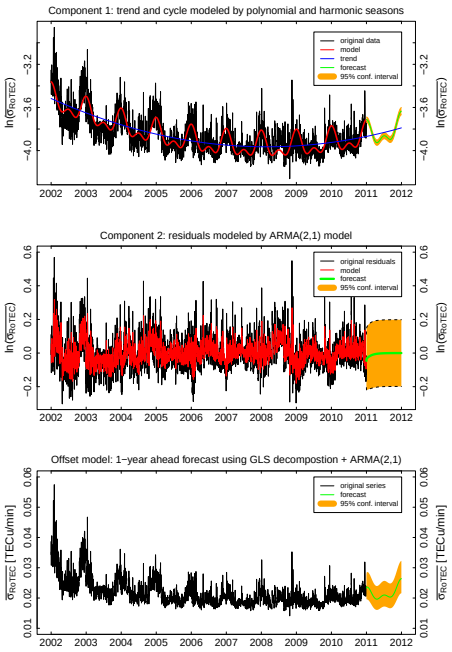


Figure 8: Model (2002-2010) and forecast (2011) of the offset series. *Upper panel*: trend and cycle are fitted by using generalized least-squares (GLS) procedure, which features harmonic seasons and a second order polynomial for the trend. *Middle panel*: residuals from this fit are modeled by autoregressive and moving average (ARMA) method. *Bottom panel*: offset model is constituted by summing the two above-mentioned components.

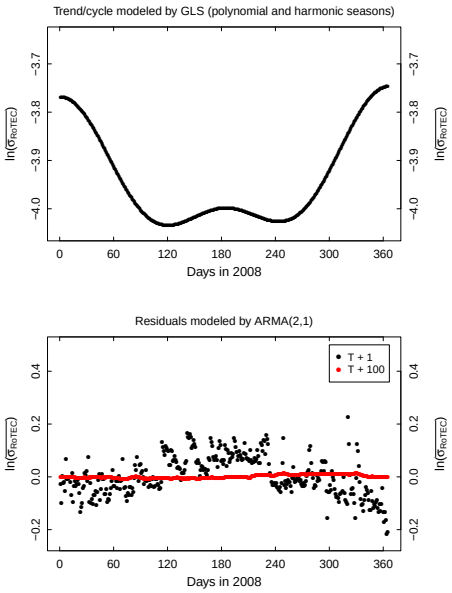


Figure 9: *Top panel*: determinist forecast of trend/cycle component for year 2008. *Bottom panel*: residual forecast using ARMA(2,1) model for prediction steps T+1 and T+100.

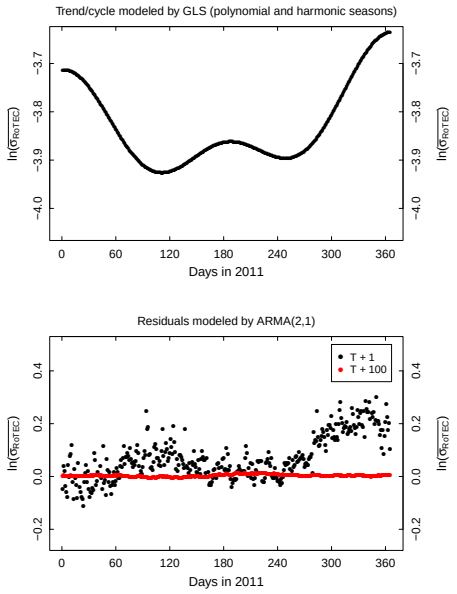


Figure 10: *Top panel*: determinist forecast of trend/cycle component for year 2011. *Bottom panel*: residual forecast using ARMA(2,1) model for prediction steps T+1 and T+100.

around zero. In addition, analysis of total and partial autocorrelograms reveals the presence of autocorrelation within the series. Therefore, an autoregressive and moving average (ARMA) method is used to fit the residual series. This algorithm implies not only autoregressive terms, as used for trend/cycle modeling in the previous paragraph, but also moving average terms whose effects correspond to a smoothing of the error modeling and a better fitting than with a pure autoregressive model. Once again, all details about the implementation and the computation can be found in Box and Jenkins (1976); Brockwell and Davis (2002). The physical meaning of the autoregressive terms in residual model lies in the presence of relatively long-lived phenomena lasting several days. For instance, the presence of a given sunspot group rises TEC values due to an enhancement of EUV and soft X-rays. This leads to a larger TEC background, which implies larger amplitudes of ionospheric irregularities. Another likely cause of strong autocorrelation lies in a specific tropospheric system responsible for the generation of atmospheric gravity waves detected in the ionosphere as traveling ionospheric disturbances (Bertin et al., 1978; Beer, 1974; Lastovicka, 2006).

Residual time series modeling consists in computing several ARMA candidate models, each of them being characterized by a given order for autoregressive and moving average terms. Then, we compare the different models on the basis of the Akaike Information Criterion (AIC), which is an indicator of the goodness of the fit. The candidate presenting the lower AIC becomes the selected model, except if another candidate gives a similar AIC value with smaller orders, in which case the latter is chosen.

The ARMA model selected is an ARMA(2,1), what means that the autoregressive component is of order 2 (*i.e.* previous two days influence) and the moving average component is of order 1. It is depicted in figure 8, where forecast values for year 2011 are also presented. As we can observe, forecast values tend quickly to zero, which is due to the fact that the influence of last days of 2010 vanishes with time. A more detailed analysis of the ARMA model is presented in the next section where validation dataset (*i.e.* data relative to years 2008 and 2011) have been taken into account.

Finally, we get the offset model by summing both GLS and ARMA models and then applying an exponential transformation to retrieve the original units. Forecast values and their corresponding confidence interval for year 2011 are shown in figure 8. Let us note that the most important contribution to the final model confidence interval is coming from the residual modeling.

### *3.4. Validation*

This section aims to validate the final model, called climatological model, made up of PCA and offset models (see figure 2). As the validation dataset covers two periods (2008 for solar minimum and 2011 for active conditions), we have to compare two forecasts with their related true values. These forecasts, featuring a time resolution of 15 minutes, have been computed for prediction steps (*i.e.* future epochs) of 1 day (T+1) and 100 days (T+100). As PCA and trend/cycle models do not depend on prediction step, difference between epochs T+1 and T+100 lies in the ARMA component. In figures 9 and 10 we present ARMA residual forecasts for prediction steps T+1 and T+100. Considering T+100, we can observe that ARMA forecast is not markedly different from zero for both 2008 and 2011. For this timestep one can therefore state that ARMA model does not provide any added value to the climatological model. Conversely, forecast values are significantly different from zero considering the T+1 timestep. For year 2008, ARMA model lowers the forecast values until day 100 (spring equinox). Then, it tends to increase the forecast during the whole summer and finally to lower again at the end of 2008 (fall and winter). From these observations we can conclude that trend/cycle model underestimates summer $\overline{\sigma_{RoTEC}}$ values and overestimates the winter behavior. This latter point is certainly due to the fact that, according to the

trend/cycle model, a new solar cycle should have appeared around August 2008. In practice, this did not happen and residual values tend to remain negative. In that sense, the ARMA residual model can be considered as an adaptive model. Considering year 2011, similar observations can be made: ARMA forecast tend to adapt the residual level, especially in fall and winter where the trend/cycle model clearly underestimates $\overline{\sigma_{RoTEC}}$ values.

Validation of the climatological model can also be done through the computation of the root mean square (RMS) of differences between observations and forecast values for years 2008 and 2011. Absolute RMS is computed daily and is expressed as follows:

$$RMS_i = \sqrt{\langle (X_{ij} - M_{ij})^2 \rangle} \tag{10}$$

with

$i$ the day identifier, from 1 to 365;

$X_{ij}$ the observation for day $i$ at epoch $j$;

$M_{ij}$ the model value for day $i$ at epoch $j$.

Relative RMS values are obtained by dividing absolute RMS by the daily mean of absolute $\overline{\sigma_{RoTEC}}$ values. Both relative and absolute values are depicted in figure 11 where prediction steps T+1 and T+100 have been represented. From the previous conclusions, we can consider that T+100 RMS values correspond to a PCA + trend/cycle model, without any residual modeling.

The common feature between the four graphs of figure 11 lies in a larger RMS in winter than in summer. Typically, relative RMS is around 10-15% in summer for both solar conditions (2008 and 2011). During winter, this value oscillates around 20-25% during solar minimum, reaching rarely more than 40%. Under active conditions (2011), RMS values oscillate also around 25% but with a larger variability than for solar minimum, exhibiting up to 60%. As explained above, the main difference between T+1 and T+100 is due to residual modeling. ARMA model allows to improve the model accuracy during summer and for the end of the year, where it brings corrections for a too optimistic trend/cycle model in 2008 and a too pessimistic trend/cycle model in 2011. Translated into relative RMS, figure 11 shows that, for end of 2008, values stay around 25% for T+1 model while they can exceed 35 or 40% when no ARMA model is considered. In 2011, mean RMS values oscillate around 30-35% in winter when the T+100 model is taken into account.

Residual model using the ARMA method is therefore a convenient way to make the final model adaptive to current conditions if the prediction step is not too far from the last observed epoch. We can assess the added value of residual modeling through computing the yearly average of daily RMS for different timesteps. More particularly, we have considered the prediction steps from T+1 to T+100 and we have observed that residual modeling was null on average for the latter case. Results, depicted in figure 12, show that mean RMS significantly increases in the first four or five days, after which it tends to an asymptotic RMS value due to the only deterministic part of the model. From this figure, we can state that the climatological model reliability is about four or five days, being the timestep from which the ARMA contribution tends to be negligible. It is worth adding that the mean RMS values are larger for year 2011 than for 2008 due to the larger RMS values observed during fall and winter. Moreover, we can also observe from figure 12 that the convergence speed during 2011 is slower than for 2008. This behavior is most probably due to a larger influence of the residual modeling in 2011.

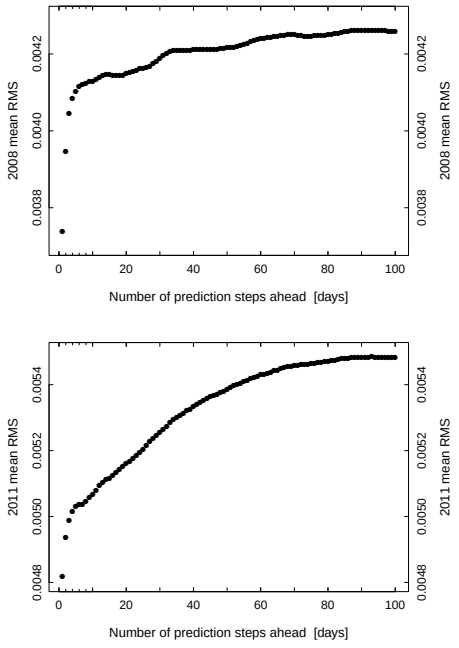


Figure 12: Yearly mean of daily RMS values for prediction steps T+1 to T+100 days for years 2008 (top) and 2011 (bottom).

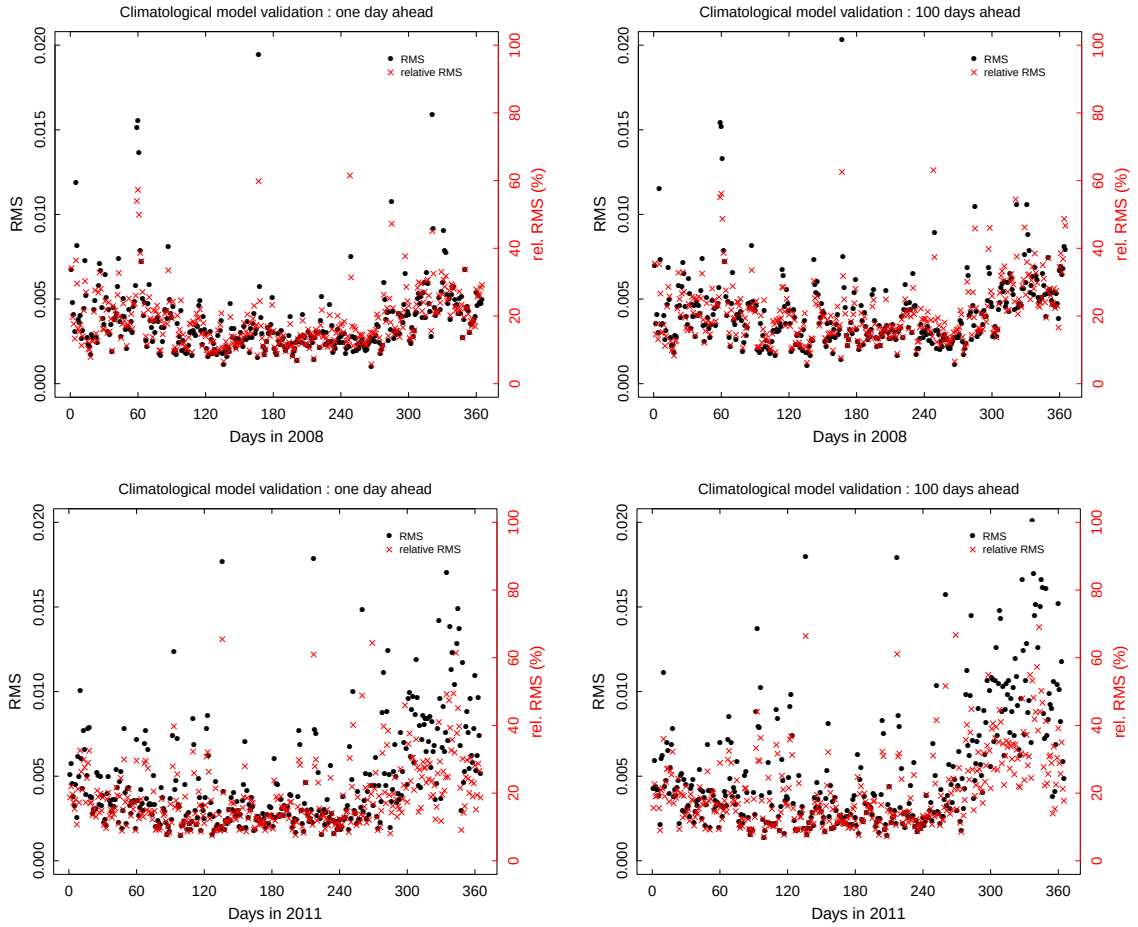


Figure 11: Validation of climatological model. Absolute (*dots*) and relative (*crosses*) RMS values for years 2008 (top) and 2011 (bottom) are shown for a prediction step of 1 day (*left panel*) and 100 days (*right panel*).

## 4. Discussion and perspectives

We have presented a climatological model of ionospheric irregularities valid for the Belgian region. This model does not consider transient events due to disturbed space weather conditions, such as geomagnetic storms or solar flares. For operational forecasting, geomagnetic activity has to be taken into account as these disturbed conditions are part of the observations from which the model is build. On the one hand, residuals modeled by ARMA will reflect the increase in ionospheric activity due to active conditions and the model will therefore undergo an increase in its offset value. This is true when considering geomagnetic storms whose time span can extend up to several days. On the other hand, ARMA(2,1) is certainly not the best model to describe rapid changes in ionospheric plasma induced by space-weather events. Indeed, the offset model has a daily time resolution while time scale of space-weather events can be significantly shorter than one day. In this context, a specific space weather model with a time resolution of about one hour should be developed and added to the climatological model for real-time forecasting.

In the offset model, solar cycle influence has been modeled by a second order polynomial. If this model gives satisfactory results while considering the time span analyzed in this paper, it could not be the case during solar maximum periods. For real-time modeling and forecasting, several mathematical functions should be tested to better capture the solar cycle influence on ionospheric irregularity occurrence.

The main drawback of a climatological model is its continuity: indeed it does not characterize inter-daily variability at all. Moreover, it does not provide any explanation about the difference between winter and sum-

mer behaviors as the model is purely statistical. The next step is to develop a semi-empirical model still based on statistics but which can assimilate information coming from proxies of ionospheric irregularities. Such proxies can probably be found in neutral part of the atmosphere, which is responsible for the generation of atmospheric gravity waves observed in the ionosphere (Bertin et al., 1978; Artru et al., 2005; Lastovicka, 2006). For instance, some meteorological observations as wind speed around tropopause (jet stream height) could exhibit a good agreement with winter irregularity occurrence. As a consequence, wind speed forecasts given by meteorological models could be used to modulate the climatological forecast background. Future developments in forecasting methods should certainly be thought in that way.

Finally, as the area of applicability of the climatological model is limited to the Belgian region, some additional validation over other mid-latitude stations should be achieved to make the model applicable to the whole mid-latitude region.

## 5. Conclusions

Ionospheric irregularities represent a important threat for GPS high-precision positioning techniques, used mainly by surveyors, civil engineers and farmers. To monitor and forecast this activity, a climatological model has been set up on the basis of an irregularities time series in Belgium between 2002 and 2011. This local model is divided into two main components.

The first models daily variability of irregularities. Resulting from a statistical method called principal component analysis (PCA), it allows to reproduce the main patterns of the time series that has a time resolution of 15 minutes. Among them are the activity maximum observed during winter days and the slight maximum during nighttime in summer. As the PCA model shows a null daily average, it has to be leveled by the offsets, which correspond to daily mean values. This series, whose behavior describes solar cycle and seasonal influences on ionospheric irregularities occurrence, is the second component of the model. It has been modeled by a quadratic trend and harmonic seasons, computed together in a generalized least-squares (GLS) adjustment. Residuals are fitted by an ARMA(2,1) model, which is a statistical autoregressive model. In this context, ARMA allows to correct GLS forecast values by taking into account the previous residual values.

The climatological model, constituted by adding both PCA and offset models, has been validated on the whole years 2008 and 2011. Its accuracy, expressed in terms of RMS, depends on the season: more particularly, it is lower during winter. Moreover, the added value of ARMA modeling has been assessed: the use of the ARMA method significantly improves the forecast up to four or five days after the last observation, epoch from which its contribution can be considered as negligible.

In the future, several model improvements should be considered. First, the solar cycle modeling function, which corresponds at the present time to a second order polynomial, may take another form, depending on the solar cycle phase considered. Another major improvement would be the addition of a space-weather component, what will allow to take into account the ionospheric irregularities due to transient events such as geomagnetic storms or solar flares. Finally, the development of another model should be based on proxy assimilation: by making the model semi-empirical, it could help to improve the inter-daily variability mainly driven by neutral atmospheric behavior.

## References


Artru, J., Ducic, V., Kanamori, H., Lognonne, P., Murakami, M., 2005. Ionospheric detection of gravity waves induced by tsunamis. Geophysical Journal International 160, 840–848.

Beer, T., 1974. Atmospheric waves. Adam Hillger, London.

Bertin, F., Testud, J., Kersley, L., Rees, P., 1978. The meteorological jet stream as a source of medium scale gravity waves in the thermosphere: an experimental study. Journal of Atmospheric and Solar–Terrestrial Physics 40, 1161–1183.

Box, G. E., Jenkins, G. M., 1976. Time Series Analysis: Forecasting and Control. Holden-Day.

Brockwell, P. J., Davis, R. A., 2002. Introduction to Time Series and Forecasting. Springer.

Collier, A. B., 2009. Principal component analysis of sub-ionospheric propagation conditions. In: International Conference on Ionospheric Radio Systems and Techniques (IRST). The Institution of Engineering and Technology (IET), Edinburgh, UK, pp. 86–90.

Cowpertwait, P. S., Metcalfe, A. V., 2009. Introductory Time Series with R. Springer.

Davies, K., 1990. Ionospheric radio. Peter Peregrinus Ltd., London.

Georges, T., 1968. Hf doppler studies of traveling ionospheric disturbances. Journal of Atmospheric and Terrestrial Physics 30, 735–746.

Hernandez-Pajares, M., Juan, J., Sanz, J., 2006. Medium-scale traveling ionospheric disturbances affecting GPS measurements: spatial and temporal analysis. Journal of Geophysical Research 111 (A07S11).

Hocke, K., Schlegel, K., 1996. A review of atmospheric gravity waves and travelling ionospheric disturbances: 1982–1995. Annales Geophysicae 14, 917–940.

Hofmann-Wellenhof, B., Lichtenegger, H., Collins, J., 2001. GPS theory and practice, fifth, revised edition Edition. Springer-Verlag, Wien.

Hunsucker, R. D., 1982. Atmospheric gravity waves generated in the high-latitude ionosphere: A review. Reviews of Geophysics 20, 293–315.

Kotake, N., Otsuka, Y., Tsugawa, T., Ogawa, T., Saito, A., 2006. Climatological study of GPS total electron content variations caused

by medium-scale traveling ionospheric disturbances. Journal of Geophysical Research 111 (A04306).

Kouris, S. S., Polimeris, K. V., Romano, V., Zolesi, B., Cander, L. R., 2006. Within-the-hour variability: levels and their probabilities. Annals of Geophysics 49, 945–959.

Kutiev, I., Muhtarov, P., Cander, L. R., Levy, M. F., 1999. Short-term prediction of ionospheric parameters based on auto-correlation analysis. Annali di Geofisica 42 (1), 121–127.

Lastovicka, J., 2006. Forcing of the ionosphere by waves from below. Journal of Atmospheric and Solar–Terrestrial Physics 68, 479–497.

Leick, A., 2004. GPS satellite surveying, third edition Edition. John Wiley & sons, Inc., Hoboken, New Jersey.

Lejeune, S., Warnant, R., 2008. A novel method for the quantitative assessment of the ionosphere effect on high accuracy GNSS applications, which require ambiguity resolution. Journal of Atmospheric and Solar–Terrestrial Physics 70, 889–900.

Lejeune, S., Wautelet, G., Warnant, R., 2012. Ionospheric effects on relative positioning within GPS dense network. GPS Solutions 16 (1), 105–116.

Muhtarov, P., Kutiev, I., 1999. Autocorrelation method for temporal interpolation and short-term prediction of ionospheric data. Radio Science 34 (2), 459–464.

Rishbeth, H., 2006. F–region links with the lower atmosphere? Journal of Atmospheric and Solar–Terrestrial Physics 68, 469–478.

Warnant, R., Pottiaux, E., 2000. The increase of the ionospheric activity as measured by GPS. Earth Planets Space 52, 1055–1060.

Wautelet, G., Lejeune, S., Warnant, R., 2009. Effects of ionospheric small-scale structures on GNSS. In: International Conference on Ionospheric Radio Systems and Techniques (IRST). The Institution of Engineering and Technology (IET), Edinburgh, UK, pp. 196–200.

Wintoft, P., Cander, L. R., 2000. Twenty-four hour predictions of fOF2 using time delay neural networks. Radio Science 35 (2), 395–408.

Xu, G., 2003. GPS Theory, algorithms and applications. Springer-Verlag, Berlin Heidelberg New York.